Compton profile – the projection of the electron momentum density distribution onto the X-ray scattering vector – can be isolated from the relativistic differential scattering cross section within the impulse approximation. Several experimental and theoretical investigations have been concerned with understanding the changes in the spectral distribution when electron binding energies cannot be discounted. It has been found (*e.g.* Pattison & Schneider, 1979; Bloch & Mendelsohn, 1974) that, to a high degree of accuracy, the spectral distribution is merely truncated at energy transfers $E \leq E_B$.

This has led to the suggestion that the incoherent intensity can be obtained by integrating the spectral distributions, *i.e.* from

$$\frac{\mathrm{d}\sigma}{\mathrm{d}\Omega} = \int_{E_1 - E_B}^{\infty} \frac{\mathrm{d}^2\sigma}{\mathrm{d}\Omega\,\mathrm{d}E_2}\,\mathrm{d}E_2. \qquad (7.4.3.6)$$

Unfortunately, this requires the Compton profile of each electron shell as input [Compton line shapes have been tabulated by Biggs, Mendelsohn & Mann (1975)] for all elements.

Ribberfors (1983) and Ribberfors & Berggren (1982) have shown that this calculation can be dramatically simplified, without loss of accuracy, by crudely approximating the Compton line shape. Fig. 7.4.3.2 shows the incoherent scattering from aluminium, modelled in this way, and compared with experiment, Waller–Hartree theory, and an exact integral of the truncated impulse Compton profile.

7.4.3.4. *Plasmon, Raman, and resonant Raman scattering*

In typical X-ray experiments, as is evident from Table 7.4.3.1, the energy transfer may be so low that Compton scattering will be inhibited from all but the most loosely bound electrons. Indeed, in the situation in metals where $\mathbf{K}$, the momentum transfer, is less than $\mathbf{k}_F$ (the Fermi momentum), Compton scattering from the conduction electrons may be restricted by exclusion because of the lack of unoccupied final states [see Bushuev & Kuz'min (1977)]. Fortunately, in these uncertain circumstances, the incoherent intensities are low. In this regime, the electron gas may be excited into collective motion. For almost all solids, the plasmon excitation energy is 20–30 eV and, in the random phase approximation, the incoherent scattering factor becomes $S(\Delta E, K) \propto (K^2/w_p)\delta(\Delta E - h\omega_p)$, where ω_p is the plasma frequency.

At slightly higher energies ($\Delta E \geq E_B$), Compton scattering and Raman scattering can coexist, though the Raman component is only evident at low momentum transfer (Bushuev & Kuz'min, 1977). The resultant spectrum is often referred to as the Compton–Raman band. In semi-classical radiation theory, Raman scattering is usually differentiated from Compton scattering by dropping the requirement for momentum conservation between the photon and the individual target electron, the recoil being absorbed by the atom. The Raman band corresponds to transitions into the lowest unoccupied levels and these can be calculated within the dipole approximation as long as $|\mathbf{K}|a < 1$, where $\mathbf{K}$ is the momentum transfer and a the orbital radius of the core electron undergoing the transition. The transition probability in equation (7.4.3.4) becomes

$$\sum_f |\langle\psi_f|\mathbf{r}|\psi_i\rangle|^2 \delta(E_f - E_i - \Delta E), \qquad (7.4.3.7)$$

which implies that the near-edge structure is similar to the photoelectric absorption spectrum.

Whereas plasmon and Raman scattering are unlikely to make dramatic contributions to the total incoherent intensity, resonant Raman scattering (RRS) may, when $E_1 \leq E_B$. The excitation involves a virtual K-shell vacancy in the intermediate state and a vacancy in the L (or M or N) shell and an electron in the continuum in the final state. It has now been observed in a variety of materials [see, for example, Sparks (1974), Eisenberger, Platzman & Winick (1976), Schaupp *et al.* (1984)]. It was predicted by Gavrila & Tugulea (1975) and the theory has been treated comprehensively by Åberg & Tulkki (1985). The effect is the exact counterpart, in the inelastic spectrum, of anomalous

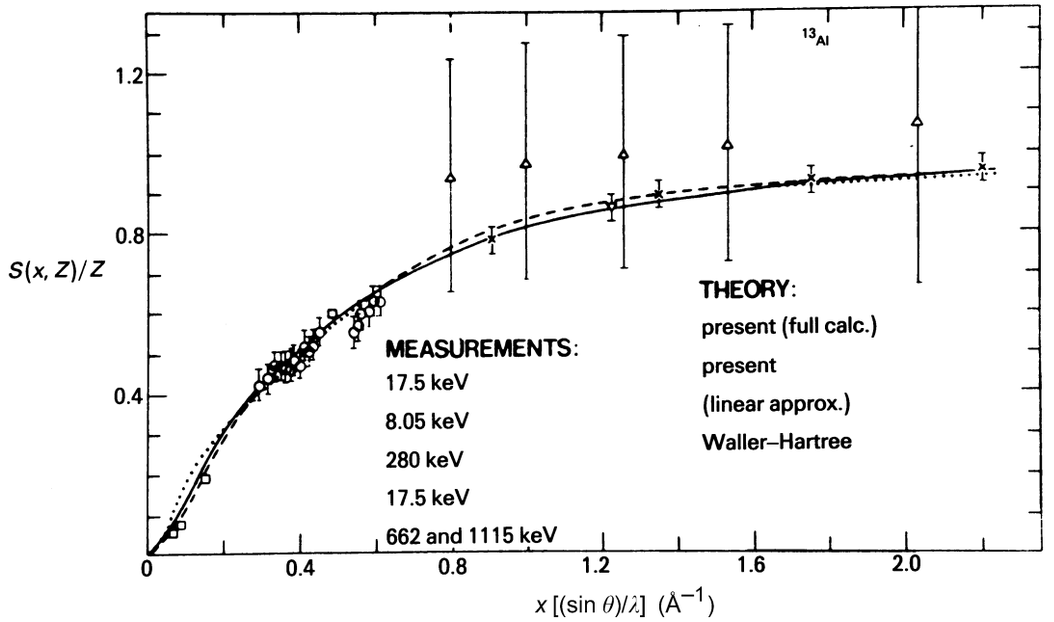

Fig. 7.4.3.2. The incoherent scattering function, $S(x, Z)/Z$, per electron for aluminium shown as a function of $x = (\sin\theta)/\lambda$. The Waller–Hartree theory (·····) is compared with the truncated impulse approximation in the tabulated Compton profiles (Biggs, Mendelsohn & Mann, 1975) cut-off at $E < E_B$ for each electron group (——). The third curve (– – –) shows the simplification introduced by Ribberfors (1983) and Ribberfors & Berggren (1982). The predictions are indistinguishable to within experimental error except at low $(\sin\theta)/\lambda$. Reference to the measurements can be found in Ribberfors & Berggren (1982).

Copyright © 2006 International Union of Crystallography

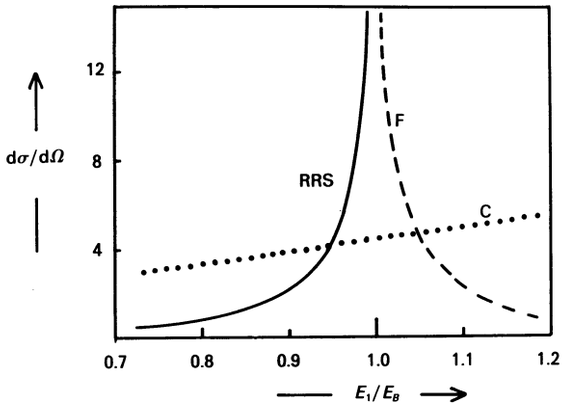

Fig. 7.4.3.3. The cross section for resonant Raman scattering (RRS) and fluorescence (F) as a function of the ratio of the incident energy, E, and the K-binding energy, E_B. The units of $d\sigma/d\Omega$ are $(e^2/mc^2)^2$ and the data are taken from Bannett & Freund (1975). For comparison, the intensity of Compton scattering (C) from copper through an angle of 30° is also shown [data taken from Hubbell *et al*. (1975)].

scattering in the elastic spectrum. It is important because, as the resonance condition is approached, the intensity will exceed that due to Compton scattering and therefore play havoc with any corrections to total intensities based solely on the latter.

Although systematic tabulations of resonance Raman scattering do not exist, Fig. 7.4.3.3, which is based on the calculations of Bannett & Freund (1975), shows how the intensity of RRS clearly exceeds that of the Compton scattering for incident energies just below the absorption edge. However, since the problems posed by anomalous scattering and X-ray fluorescence are generally appreciated, the energy range $0.9 < E_1/E_B < 1.1$ is wisely avoided by crystallographers intent upon absolute intensity measurements.

7.4.3.5. *Magnetic scattering*

Finally, and for completeness, it should be noted that the intensity of Compton scattering from a magnetic material with a net spin moment will, in principle, differ from that from a non-magnetic material. For unpolarized radiation, the effects are only discernible at photon energies greatly in excess of the electron rest mass energy, $mc^2 = 511\,\text{keV}$, but for circularly polarized radiation effects at the 1% level can be found in Compton scattering experiments carried out at $E_1 \simeq 1/10\,mc^2$ on ferromagnets such as iron. See Lipps & Tolhoek (1954) for a comprehensive description of polarization phenomena in magnetic scattering and Lovesey (1993) for an account of the scattering theory.

7.4.4. White radiation and other sources of background (By P. Suortti)

7.4.4.1. *Introduction*

By definition, the background includes everything except the signal. In an X-ray diffraction measurement, the signal is the pattern of Bragg reflections. The profiles of the reflections should be determined by the structure of the sample, and so the broadening due to the instrument should be considered as background. In the ideal angle-dispersive experiment, a well collimated beam of X-rays having a well defined energy (and a polarization, perhaps) falls on the sample, and only the radiation scattered by the sample is detected. Furthermore, the detector should be able to resolve all the components of scattering by energy, so that each scattering process could be studied separately. It is obvious that only after this kind of analysis are the Bragg reflections (plus the possible disorder scattering) unequivocally separated from the background arising from other processes. In most cases, however, this analysis is not feasible, and the reflections are separated by using certain assumptions concerning their profile, and the success of this procedure depends on the peak-to-background ratio.

The ideal situation described above is all too often not encountered, and experimenters are satisfied with too low a level of resolution. The aim of the present article is to point out the sources of the unwanted and unresolved components of the registered radiation and to suggest how these may be eliminated or resolved, so that the quality of the diffraction pattern is as high as possible. The article can cover only a few of the possible experimental situations, and only the 'almost ideal' angle-dispersive instrument is considered. It is assumed that the beam incident on the sample is monochromatized by reflection from a crystal and that the scattered radiation is registered by a low-noise quantum detector, which is the standard arrangement for modern diffractometers. Filtered radiation and photographic recording are used in certain applications, but these are excluded from the following discussion. The wavelength-dispersive or Laue methods are becoming popular at the synchrotron-radiation laboratories, and a short comment on these techniques will be included. Other sections of this volume deal with the components of scattering that are present even in the ideal experiment: thermal diffuse scattering (TDS), Compton and plasmon scattering, fluorescence and resonant Raman scattering, multiple scattering (coherent and incoherent), and disorder scattering.

The rest of the background may be termed 'parasitic' scattering, and it arises from three sources:

(1) impurities of the incident beam;
(2) impurities of the sample;
(3) surroundings of the sample.

Parasitic scattering is occasionally mentioned in the literature, but it has hardly ever been the subject of a detailed study. Therefore, the present article will discuss the general principles of the minimization of the background and then illustrate these ideas with examples. Most of the discussion will be directed to the first of the three sources of parasitic scattering, because the other two depend on the details of the experiment.

7.4.4.2. *Incident beam and sample*

An ideal diffraction experiment should be viewed as an X-ray optical system where all the parts are properly matched for the desired resolution and efficiency. The impurities of the incident beam are the wavelengths and divergent rays that do not contribute to the signal but scatter from the sample through the various processes mentioned above. The propagation of the X-ray beam through the instrument is perhaps best illustrated by the so-called phase-space analysis. The three-dimensional version, which will be used in the following, was introduced by Matsushita & Kaminaga (1980) and was elaborated further by Matsushita & Hashizume (1983). The width, divergence and wavelength range of the beam are given as a contour diagram, which originates in the X-ray source, and is modified by slits, monochromator, sample, and the detection system. The actual five-dimensional diagram is usually given as three-dimensional projections on the plane of diffraction and on the plane perpendicular to it and the beam axis, and in most cases the first projection is sufficient for an adequate description of the geometry of the experiment.